Editors' Suggestion

Laser-assisted electron-atom radiative recombination in short laser pulses

Deeksha Kanti,[1] J. Z. Kamiński,[1] Liang-You Peng,[2,3,4,*] and K. Krajewska[1,†]

[1]*Institute of Theoretical Physics, Faculty of Physics, University of Warsaw, Pasteura 5, 02-093 Warsaw, Poland*

[2]*State Key Laboratory for Mesoscopic Physics and Frontiers Science Center for Nano-optoelectronics, School of Physics, Peking University, Beijing 100871, China*

[3]*Beijing Academy of Quantum Information Sciences, Beijing 100193, China*

[4]*Collaborative Innovation Center of Extreme Optics, Shanxi University, Taiyuan 030006, China*

(Received 14 July 2021; accepted 31 August 2021; published 20 September 2021)

A comprehensive theoretical treatment of laser-assisted electron-atom radiative recombination in the presence of short laser pulses is presented. Our formulation lacks various unphysical effects observed in previous works, such as oscillations and high-energy tails in the spectrum of emitted radiation; however, it accounts for a contribution from the field-free process. As a result, the energy distribution of emitted radiation consists of a point spectrum embedded in a continuum. We demonstrate that the features of the latter are determined by the laser field. For instance, in the case of a train of pulses, comb structures appear in the radiation spectrum. We attribute them to constructive interference between probability amplitudes of recombination assisted by each pulse from the train. Finally, we show that the vector potential describing the laser field is encoded in the spectrogram of emitted radiation. This suggests the use of the spectrogram for a complete temporal reconstruction of the laser field, irrespective of whether it is an isolated pulse or a pulse train.

DOI: 10.1103/PhysRevA.104.033112

I. INTRODUCTION

Electron recombination by an atomic target, which occurs in the presence of a strong laser field, is of fundamental importance for the development of strong-field physics and related areas such as attoscience. The point is that laser-assisted radiative recombination (LARR) is the underlying mechanism of high-order harmonic generation (HHG), which has played a pivotal role in the development of nonlinear optics. It has been proposed [1,2] that ionized electrons can be returned to the ionized core by an oscillating laser field and recombine, thus releasing the harmonics that are multiples of the laser photon energy. Due to their phase coherence, a proposal to synthesize the HHG spectrum into attosecond pulses of light has been put forward [3,4]. Currently, attosecond pulses are routinely generated in laboratories worldwide and find interesting applications in atomic and molecular physics as well as in nanotechnology (for recent reviews, see Refs. [5–7]). At this point, we would like to mention that there is a fundamental difference between laser-assisted recombination and high-order harmonic generation. In LARR the incident electron momentum can be arbitrary, while in HHG this momentum is determined by the first two steps of the above-described three-step mechanism. In addition, while LARR is a laser-assisted process, HHG is induced by a laser field, which makes a significant difference in treating them quantum mechanically, as described in Sec. II.

The ability to generate intense and coherent light with controllable properties is one of the most inspiring achievements of the previous century. Arguably, LARR lies at the heart of the development of nonlinear optics and laser technology. For this reason, it has been a topic of numerous investigations. Except for experimental works such as [8–12], a majority of them concerned theoretical aspects of LARR and the effect of an external laser field on the properties of emitted radiation. Essentially, radiative recombination can occur in the absence of an external field. Thus, the influence of monochromatic [13–23] and multicolor [24–28] plane-wave laser fields was investigated and suggested as a means to control the LARR spectrum. Most recent investigations have focused on radiative recombination in the presence of short laser pulses [29–34], which provide an additional manner of laser control. Aspects such as carrier-envelope phase effects and the influence of pulse duration on the spectra of laser-assisted recombination radiation have been analyzed, hence shining additional light on the properties of HHG.

In this paper we further analyze the laser-field aspects of the LARR process. For clarity, we focus on electron-atom recombination, which involves a short-range atomic interaction. Note that historically such a process is called laser-assisted radiative attachment. Since recombination is a more general term as it covers various scenarios in which the recombining electron transfers its energy and momentum to a third body, we use it throughout the paper. In our case, it is justified to work in the framework of the strong-field approximation (SFA), as introduced by Keldysh [35], Faisal [36], and Reiss [37]. In this approximation, the influence of the atomic potential on the initial electron scattering state is neglected while the laser field is neglected for the final

*liangyou.peng@pku.edu.cn

†Katarzyna.Krajewska@fuw.edu.pl

 ©2021 American Physical Society

bound electron. Most importantly, we develop a comprehensive theoretical approach to describe LARR, which explicitly accounts for contributions from the field-free and the field-modified processes. This is in contrast to previous works where the bandwidth-limited probability amplitude of LARR was calculated. Also, we consider an initial electron wave packet with momentum distribution that allows smearing of the field-free divergence. While our theory accounts for an arbitrary laser field, we illustrate it for isolated pulses and pulse trains. We observe a coherent enhancement of the LARR spectra for the latter. More specifically, the comb structures in the spectra appear with an intensity that scales quadratically with the number of pulses in a train. This ensures synthesis of the laser-assisted recombination radiation into short pulses, similar to the proposal of Refs. [3,4] (see also Refs. [30,31] in the context of LARR). Another aspect of our investigation relates to temporal reconstruction of the laser field. More specifically, our time-frequency analysis of the LARR spectra demonstrates the possibility of *in situ* measurement of the laser field. The method is insensitive to the parameters of the field and can be used for the metrology of both isolated pulses and pulse trains, therefore proving its great versatility.

The paper is organized as follows. In Sec. II we formulate the theoretical framework of laser-assisted radiative recombination. We start our consideration by analyzing the case of a monochromatic electron wave in the initial state (Sec. II A), which then is generalized to account for coherent superposition of such waves (Sec. II B). For completeness, in Sec. II C we provide simplified formulas which are based on the bandwidth-limited probability amplitude. The electron-wave-packet model and the laser-field model used in our paper are introduced in Secs. II D and II E, respectively. The energy distributions of laser-assisted recombination radiation are calculated numerically according to our comprehensive approach and the simplified one in Sec. III A. While the results discussed there are for isolated laser pulses, in Sec. III B we present the LARR energy spectra for pulse trains. As a follow-up, in Sec. III C we perform a time-frequency analysis of our results. The proposal to use the time-frequency analysis for *in situ* measurement of the laser field is put forward in Sec. III D. Finally, we summarize our results and give prospects for further investigations in Sec. IV. More details on derivations are given in the Appendices.

In our numerical analysis we use the atomic units of momentum $p_0 = \alpha m_e c$, energy $E_0 = \alpha^2 m_e c^2$, length $a_0 = \hbar/p_0$, time $t_0 = \hbar/E_0$, electric-field strength $\mathcal{E}_0 = \alpha^3 m_e^2 c^3/|e|\hbar$, and laser-field intensity $I_0 = \epsilon_0 c \mathcal{E}_0^2 \approx 7.02 \times 10^{16}$ W/cm^2, where m_e and $e = -|e|$ are the electron rest mass and charge, respectively, α is the fine-structure constant, and $\epsilon_0 = e^2/4\pi\alpha\hbar c$ is the vacuum permittivity. In analytical formulas, on the other hand, we set $\hbar = 1$ while explicitly keeping the remaining fundamental constants.

II. THEORETICAL FORMULATION

Processes which occur in a laser field can be identified as either laser induced or laser assisted. To mention a few examples, ionization and high-order harmonic generation are among laser-induced processes, whereas laser-assisted radiative recombination and scattering belong to the second group. Such a distinction originates from the fact that laser-induced processes occur only in the presence of the field, while laser-modified processes can occur irrespective of it. Note that properties of the latter are significantly modified by the laser field.

The probability amplitude of a quantum process can always be represented as a time integral, which follows from a relevant dynamical equation such as the Schrödinger equation in nonrelativistic quantum mechanics. Unfortunately, the explicit form of the integral is typically not known and one has to rely on approximations, with the SFA being one of the most commonly used in the area of strong-field physics. Irrespective of approximations, the analysis of the time integral for laser-induced and laser-assisted processes that occur in a finite laser field is different. Assume that the field lasts within the finite-time interval from t_i to t_f. For laser-induced processes, the corresponding time integral can be simply reduced to the interval $[t_i, t_f]$; otherwise the integrand is zero. However, for laser-assisted processes this is not the case. The reason is that laser-assisted processes occur irrespective of the field and hence the integrand defining the probability amplitude is nonzero also for times $t < t_i$ and $t > t_f$. Thus, the integration limits cannot be restricted in this case to the interval $[t_i, t_f]$. In fact, restricting the integration limits is equivalent to introducing an artificial cutoff of the integrand, which results in the so-called Gibbs effect [38,39]. The latter leads to the appearance of unphysical oscillations of the probability distributions, as can be seen in various papers on LARR (see, e.g., [32–34]). In order to avoid this problem, one has to appropriately transform the time integral. Below we illustrate how to perform such a transformation in the case of laser-assisted radiative recombination, but the same concerns other laser-assisted processes.

In the following, we present the theoretical formulation of the laser-assisted radiative electron-atom recombination followed by the formation of a H^- ion and emission of a resulting photon. The latter can in principle carry an arbitrary energy, even though it is typically considered in the context of generation of high-energy x-ray radiation. Keeping this in mind, we start our investigations by analyzing the LARR resulting from the interaction with a monochromatic electron wave.

A. LARR by the impact of a monochromatic electron wave

Consider recombination of an electron by a short-range atomic potential $V(\boldsymbol{r})$ in the presence of a laser field, thus resulting in emission of a photon. The latter is represented by a quantized electric-field operator

$$\hat{\boldsymbol{\mathcal{E}}}_{\boldsymbol{K}}(\boldsymbol{r}, t) = \hat{\boldsymbol{\mathcal{E}}}_{\boldsymbol{K}}^{(+)}(\boldsymbol{r}, t) + \hat{\boldsymbol{\mathcal{E}}}_{\boldsymbol{K}}^{(-)}(\boldsymbol{r}, t), \tag{1}$$

where

$$\hat{\boldsymbol{\mathcal{E}}}_{\boldsymbol{K}}^{(+)}(\boldsymbol{r}, t) = i\boldsymbol{\varepsilon}_{\boldsymbol{K}} \sqrt{\frac{\omega_{\boldsymbol{K}}}{2\epsilon_0 V}}\, \hat{a}_{\boldsymbol{K}} e^{-i(\omega_{\boldsymbol{K}} t - \boldsymbol{K}\cdot\boldsymbol{r})},$$

$$\hat{\boldsymbol{\mathcal{E}}}_{\boldsymbol{K}}^{(-)}(\boldsymbol{r}, t) = -i\boldsymbol{\varepsilon}_{\boldsymbol{K}} \sqrt{\frac{\omega_{\boldsymbol{K}}}{2\epsilon_0 V}}\, \hat{a}_{\boldsymbol{K}}^{\dagger} e^{i(\omega_{\boldsymbol{K}} t - \boldsymbol{K}\cdot\boldsymbol{r})}. \tag{2}$$

Here V is the quantization volume and $\hat{a}_{\boldsymbol{K}}$ and $\hat{a}_{\boldsymbol{K}}^{\dagger}$ are the annihilation and creation operators, respectively, of a photon

with energy $\omega_{\boldsymbol{K}}$, wave vector $\boldsymbol{K}$, and linear polarization $\boldsymbol{\varepsilon}_{\boldsymbol{K}}$. In the length gauge, the probability amplitude of recombination is given by

$$\mathcal{A}(\boldsymbol{p}) = -i\int_{-\infty}^{\infty} dt\,\langle\psi_B(t);1_{\boldsymbol{K}}| - e\boldsymbol{\mathcal{E}}_{\boldsymbol{K}}(\boldsymbol{r},t)\cdot\boldsymbol{r}|\psi_{\boldsymbol{p}}^{(+)}(t);0_{\boldsymbol{K}}\rangle, \tag{3}$$

where $|\psi_{\boldsymbol{p}}^{(+)}(t);0_{\boldsymbol{K}}\rangle$ describes the initial state of the system, which involves the electron carrying the momentum $\boldsymbol{p}$ in the scattering state $\psi_{\boldsymbol{p}}^{(+)}(\boldsymbol{r},t)$ and no photons, and $|\psi_B(t);1_{\boldsymbol{K}}\rangle$ is the final state of the system that describes the electron in the bound state $\psi_B(\boldsymbol{r},t)$ of energy E_B and an emitted photon. In this case, Eq. (3) becomes

$$\mathcal{A}(\boldsymbol{p}) = e\sqrt{\frac{\omega_{\boldsymbol{K}}}{2\epsilon_0 V}}\int_{-\infty}^{\infty} dt\int d^3\boldsymbol{r}\,\psi_B^*(\boldsymbol{r},t)(\boldsymbol{\varepsilon}_{\boldsymbol{K}}\cdot\boldsymbol{r}) \times\psi_{\boldsymbol{p}}^{(+)}(\boldsymbol{r},t)e^{i(\omega_{\boldsymbol{K}}t-\boldsymbol{K}\cdot\boldsymbol{r})}, \tag{4}$$

where in principle $\psi_B(\boldsymbol{r},t)$ and $\psi_{\boldsymbol{p}}^{(+)}(\boldsymbol{r},t)$ represent the exact electronic wave functions. In our calculations, we approximate them by

$$\psi_B(\boldsymbol{r},t) = e^{-iE_Bt}\psi_B(\boldsymbol{r}) \tag{5}$$

and

$$\psi_{\boldsymbol{p}}^{(+)}(\boldsymbol{r},t) = \frac{1}{\sqrt{V}}\exp\Bigg(-i\frac{\boldsymbol{p}^2}{2m_{\mathrm{e}}}t + i[\boldsymbol{p}-e\boldsymbol{A}(t)]\cdot\boldsymbol{r} + \frac{i}{2m_{\mathrm{e}}}\int_0^t d\tau[2e\boldsymbol{A}(\tau)\cdot\boldsymbol{p} - e^2\boldsymbol{A}^2(\tau)]\Bigg). \tag{6}$$

Note that Eq. (5) expresses the stationary time evolution of the atomic bound state that is not dressed by the laser field. This is justified as we are dealing in this paper with recombination assisted by short laser pulses. On the other hand, Eq. (6) describes the electron of an initial asymptotic momentum $\boldsymbol{p}$ propagating in the laser field. In other words, we neglect the influence of the atomic potential on the initial electron. Such an approximation is particularly well suited for short-range potentials, like the ones binding the negative ions. It is also a fundamental quality of the SFA [35–37], which is widely used in strong-field physics. Note that in Eq. (6), the laser field is represented by the vector potential $\boldsymbol{A}(t)$, which will be specified in Sec. III.

Next we introduce a function

$$\tilde{\Phi}_B(\boldsymbol{p}) = \int d^3\boldsymbol{r}\,\psi_B^*(\boldsymbol{r})(\boldsymbol{\varepsilon}_{\boldsymbol{K}}\cdot\boldsymbol{r})e^{i\boldsymbol{p}\cdot\boldsymbol{r}} = -i(\boldsymbol{\varepsilon}_{\boldsymbol{K}}\cdot\boldsymbol{\nabla}_{\boldsymbol{p}})\tilde{\psi}_B^*(\boldsymbol{p}), \tag{7}$$

where $\tilde{\psi}_B(\boldsymbol{p})$ denotes the Fourier transform of $\psi_B(\boldsymbol{r})$ and $\boldsymbol{\nabla}_{\boldsymbol{p}}$ is the gradient calculated with respect to the momentum coordinates. This allows us to rewrite the probability amplitude of radiative recombination (4) in the form

$$\mathcal{A}(\boldsymbol{p}) = \frac{e}{V}\sqrt{\frac{\omega_{\boldsymbol{K}}}{2\epsilon_0}}\int_{-\infty}^{\infty} dt\;\tilde{\Phi}_B(\boldsymbol{\pi}(t))e^{iQt+iH(t)}, \tag{8}$$

where we introduce the abbreviations

$$\boldsymbol{\pi}(t) = \boldsymbol{p} - e\boldsymbol{A}(t) - \boldsymbol{K}, \tag{9}$$

$$Q = E_B + \omega_{\boldsymbol{K}} - \frac{\boldsymbol{p}^2}{2m_{\mathrm{e}}}, \tag{10}$$

and

$$H(t) = \int_0^t d\tau\,h(\tau) = \int_0^t d\tau\left(\frac{e}{m_{\mathrm{e}}}\boldsymbol{p}\cdot\boldsymbol{A}(\tau) - \frac{e^2}{2m_{\mathrm{e}}}\boldsymbol{A}^2(\tau)\right). \tag{11}$$

Note that Eq. (11) implicitly defines the function $h(t)$. While Eq. (8) is very general, in order to proceed with further derivations we need to specify the final electron state. Since the SFA is particularly well suited to describe short-range bound systems, we focus on negative ions. Note, however, that derivations regarding electron-atom radiative recombination would follow the exact same path, provided the SFA were applicable in this case. Therefore, we claim that the presented method is general within the range of applicability of the SFA.

Consider an electron driven by a laser field to recombine into the ground state of a H^- ion. As demonstrated in Ref. [40], for multiphoton ionization of H^- it is the electron wave function at large distances which makes the dominant contribution to the probability amplitude. For this reason, additional effects such as polarization of an atom and electron correlations play a secondary role. Since recombination is a time-reversed process, we expect that the same argument applies in our case. Hence, following the work of Gribakin and Kuchiev [40], we assume that the ground-state wave function of H^- equals

$$\psi_B(\boldsymbol{r}) = \frac{A}{\sqrt{4\pi}}\frac{e^{-\kappa r}}{r}, \tag{12}$$

where $\kappa = \sqrt{2m_{\mathrm{e}}|E_B|} = 0.2354p_0$ and $A = 0.75\sqrt{p_0}$. Taking this into account, we derive from Eq. (7) that

$$\tilde{\Phi}_B(\boldsymbol{p}) = 4i\sqrt{\pi}A\,\frac{\boldsymbol{\varepsilon}_{\boldsymbol{K}}\cdot\boldsymbol{p}}{(\kappa^2+\boldsymbol{p}^2)^2}. \tag{13}$$

Substituting now $\tilde{\Phi}_B$ into the formula defining the probability amplitude (8), we arrive at the expression

$$\mathcal{A}(\boldsymbol{p}) = 4iA\sqrt{\frac{\pi\omega_{\boldsymbol{K}}}{2\epsilon_0}}\frac{e}{V}\int_{-\infty}^{\infty} dt\,\frac{\boldsymbol{\varepsilon}_{\boldsymbol{K}}\cdot[\boldsymbol{p}-e\boldsymbol{A}(t)]}{[\kappa^2+\boldsymbol{\pi}^2(t)]^2}e^{iQt+iH(t)}. \tag{14}$$

We will show now that this integral contains a contribution from the field-free process.

Note that we consider recombination assisted by a laser field that lasts for a short time, from 0 to T_p. This means that the vector potential defining the field $\boldsymbol{A}(t)$ is zero except for $t\in[0,T_p]$. For this reason, the integral in (14) splits into two integrals

$$\mathcal{A}(\boldsymbol{p}) = 4iA\sqrt{\frac{\pi\omega_{\boldsymbol{K}}}{2\epsilon_0}}\frac{e}{V}\left(\boldsymbol{\varepsilon}_{\boldsymbol{K}}\cdot\boldsymbol{p}\int_{-\infty}^{\infty} dt\,\frac{e^{iQt+iH(t)}}{[\kappa^2+\boldsymbol{\pi}^2(t)]^2} - \int_0^{T_p} dt\,\frac{\boldsymbol{\varepsilon}_{\boldsymbol{K}}\cdot e\boldsymbol{A}(t)}{[\kappa^2+\boldsymbol{\pi}^2(t)]^2}e^{iQt+iH(t)}\right), \tag{15}$$

with the first one needing special attention. This is reminiscent of the fact that we deal with a laser-assisted process, which happens even in the absence of the field. In the following, we will treat this integral according to the prescription introduced by Boca and Florescu in the context of Compton scattering [41], which we have adapted for our purpose in Appendix A.

Thus, using Eq. (A8), we obtain that the probability amplitude of LARR equals

$$\mathcal{A}(\boldsymbol{p}) = 4iA\sqrt{\frac{\pi\omega_{\boldsymbol{K}}}{2\epsilon_0}}\frac{e}{V}\left(2\pi\delta(Q)\frac{\boldsymbol{\varepsilon}_{\boldsymbol{K}}\cdot\boldsymbol{p}}{\left(\kappa^2+\boldsymbol{\pi}_0^2\right)^2}\right.$$
$$-\frac{\boldsymbol{\varepsilon}_{\boldsymbol{K}}\cdot\boldsymbol{p}}{Q+i\epsilon}\int_0^{T_p}dt\,\frac{F(t)}{[\kappa^2+\boldsymbol{\pi}^2(t)]^2}e^{iQt+iH(t)}$$
$$\left.-\int_0^{T_p}dt\,\frac{\boldsymbol{\varepsilon}_{\boldsymbol{K}}\cdot e\boldsymbol{A}(t)}{[\kappa^2+\boldsymbol{\pi}^2(t)]^2}e^{iQt+iH(t)}\right), \tag{16}$$

where the $i\epsilon$ prescription ($\epsilon>0$) allows us to circumvent the singularity at $Q=0$. Moreover, we recall from Appendix A that $\boldsymbol{\pi}_0\equiv\boldsymbol{\pi}(0)=\boldsymbol{p}-\boldsymbol{K}$. In addition, we write down the explicit form of the function $F(t)$,

$$F(t)=\frac{e}{m_{\rm e}}\boldsymbol{p}\cdot\boldsymbol{A}(t)-\frac{e^2}{2m_{\rm e}}\boldsymbol{A}^2(t)+4i\frac{e\boldsymbol{\mathcal{E}}(t)\cdot\boldsymbol{\pi}(t)}{\kappa^2+\boldsymbol{\pi}^2(t)}, \tag{17}$$

where, from Eq. (A4), we have substituted the definition of $h(t)$ [as it follows from Eq. (11)]. Here $\boldsymbol{\mathcal{E}}(t)=-d\boldsymbol{A}(t)/dt$ defines the laser field.

In the most general case, the emitted photon can be elliptically polarized. More specifically,

$$\boldsymbol{\varepsilon}_{\boldsymbol{K}}=\cos\delta\,\boldsymbol{\varepsilon}_{\boldsymbol{K}1}+i\sin\delta\,\boldsymbol{\varepsilon}_{\boldsymbol{K}2}, \tag{18}$$

where δ is the ellipticity parameter, whereas two linearly polarized vectors $\boldsymbol{\varepsilon}_{\boldsymbol{K}1}$ and $\boldsymbol{\varepsilon}_{\boldsymbol{K}2}$ are orthonormal, i.e., $\boldsymbol{\varepsilon}_{\boldsymbol{K}i}\cdot\boldsymbol{\varepsilon}_{\boldsymbol{K}j}=\delta_{ij}$ for $i,j\in\{1,2\}$. In light of Eq. (16), we define the partial probability amplitudes for each polarization component $\boldsymbol{\varepsilon}_{\boldsymbol{K}j}$ ($j=1,2$),

$$\mathcal{R}_j^{(0)}=A(\boldsymbol{n}_{\boldsymbol{p}}\cdot\boldsymbol{\varepsilon}_{\boldsymbol{K}j})\frac{1}{\left(\kappa^2+\boldsymbol{\pi}_0^2\right)^2}, \tag{19}$$

$$\mathcal{R}_j^{(1)}=A(\boldsymbol{n}_{\boldsymbol{p}}\cdot\boldsymbol{\varepsilon}_{\boldsymbol{K}j})\int_0^{T_p}dt\,\frac{F(t)}{[\kappa^2+\boldsymbol{\pi}^2(t)]^2}e^{iQt+iH(t)}, \tag{20}$$

$$\mathcal{R}_j^{(2)}=-A\int_0^{T_p}dt\,\frac{\boldsymbol{\varepsilon}_{\boldsymbol{K}j}\cdot e\boldsymbol{A}(t)}{[\kappa^2+\boldsymbol{\pi}^2(t)]^2}e^{iQt+iH(t)}, \tag{21}$$

where $\boldsymbol{n}_{\boldsymbol{p}}=\boldsymbol{p}/|\boldsymbol{p}|$ stands for the direction of the electron initial momentum. Introducing now the abbreviations

$$\mathcal{R}_\delta^{(\ell)}=\cos\delta\mathcal{R}_1^{(\ell)}+i\sin\delta\mathcal{R}_2^{(\ell)} \tag{22}$$

for $\ell=0,1,2$ and also

$$\mathcal{N}=4i\sqrt{\frac{\pi\omega_{\boldsymbol{K}}}{2\epsilon_0}}\frac{e}{V}=-\frac{4\pi i}{V}\sqrt{2\alpha c\omega_{\boldsymbol{K}}}, \tag{23}$$

we transform Eq. (16) into

$$\mathcal{A}(\boldsymbol{p})=\mathcal{N}\left(2\pi|\boldsymbol{p}|\delta(Q)\mathcal{R}_\delta^{(0)}-\frac{|\boldsymbol{p}|}{Q+i\epsilon}\mathcal{R}_\delta^{(1)}+\mathcal{R}_\delta^{(2)}\right). \tag{24}$$

It is interesting now to interpret this expression.

For this purpose, we use the Sokhotski-Plemelj formula

$$\frac{1}{x+i\epsilon}=\mathcal{P}\left(\frac{1}{x}\right)-i\pi\delta(x), \tag{25}$$

which allows us to distinguish in Eq. (24) two contributions of essentially different origins, namely,

$$\mathcal{A}(\boldsymbol{p})=\mathcal{A}_{\rm FM}(\boldsymbol{p})+\mathcal{A}_{\rm FI}(\boldsymbol{p}), \tag{26}$$

where the field-modified and the field-induced probability amplitudes of recombination are

$$\mathcal{A}_{\rm FM}(\boldsymbol{p})=2\pi\mathcal{N}|\boldsymbol{p}|\delta(Q)\left(\mathcal{R}_\delta^{(0)}+\frac{i}{2}\mathcal{R}_\delta^{(1)}\right), \tag{27}$$

$$\mathcal{A}_{\rm FI}(\boldsymbol{p})=\mathcal{N}\left[-\mathcal{P}\left(\frac{1}{Q}\right)|\boldsymbol{p}|\mathcal{R}_\delta^{(1)}+\mathcal{R}_\delta^{(2)}\right]. \tag{28}$$

It follows from Eqs. (17) and (20)–(22) that in the absence of the laser field $\mathcal{R}_\delta^{(1)}=\mathcal{R}_\delta^{(2)}=0$. This immediately shows that the former amplitude $\mathcal{A}_{\rm FM}(\boldsymbol{p})$ simplifies to

$$\mathcal{A}_{\rm FF}(\boldsymbol{p})=2\pi\mathcal{N}|\boldsymbol{p}|\delta(Q)\mathcal{R}_\delta^{(0)}, \tag{29}$$

which is independently derived in Appendix B for the field-free process. As it is well known, the Dirac δ function in (29) expresses the energy conservation condition. Namely, it follows from this condition that the field-free recombination occurs provided $Q=0$. In other words, in the absence of the laser field, we observe monochromatic radiation with energy

$$\omega_{\boldsymbol{K}}=\frac{\boldsymbol{p}^2}{2m_{\rm e}}+|E_B|. \tag{30}$$

With the laser field included, there is still the contribution from the field-free process [see Eq. (27)]. This time, however, it is modified by the laser field. For this reason, we refer to this process as field-modified recombination. Note that Eq. (30) is still valid in this case. In contrast, the field-induced contribution (28) vanishes in the absence of the laser field. Moreover, we have in this case the contribution from $Q\neq0$. Altogether this means that one should observe a broad spectrum of generated radiation together with the peak at $Q=0$.

So far, we have formulated the theory of laser-assisted recombination by the impact of a monochromatic electron wave. This led us to Eq. (24), which possesses a field-free singularity. Both singular distributions $\delta(Q)$ and $\mathcal{P}(\frac{1}{Q})$ can be removed, however, by considering an electron wave packet, as presented in the next section.

B. LARR by the impact of an electron coherent wave packet

Assume that initially we have a coherent electron wave packet that recombines with a hydrogen atom in the presence of a laser field. The profile of the wave packet is given by the function $f_{\boldsymbol{p}}(\boldsymbol{q})$, which is peaked around the momentum $\boldsymbol{p}$,

$$f_{\boldsymbol{p}}(\boldsymbol{q})\approx\delta^{(3)}(\boldsymbol{q}-\boldsymbol{p}). \tag{31}$$

In other words, we consider a nearly monochromatic initial electron beam. In order to generalize Eq. (4), we need to replace the scattering state $\psi_{\boldsymbol{p}}^{(+)}(\boldsymbol{r},t)$ present there by the wave packet $\psi_{\boldsymbol{p}}^{(+)}[\boldsymbol{r},t|f_{\boldsymbol{p}}]$, which functionally depends on the profile function, namely,

$$\psi_{\boldsymbol{p}}^{(+)}[\boldsymbol{r},t|f_{\boldsymbol{p}}]=\int d^3\boldsymbol{q}\,\psi_{\boldsymbol{q}}^{(+)}(\boldsymbol{r},t)f_{\boldsymbol{p}}(\boldsymbol{q}). \tag{32}$$

By doing that, we immediately realize that the probability amplitude of LARR [Eq. (4)] integrated over the initial electron momentum profile equals

$$\langle\mathcal{A}(\boldsymbol{p})\rangle=\int d^3\boldsymbol{q}\,\mathcal{A}(\boldsymbol{q})f_{\boldsymbol{p}}(\boldsymbol{q}). \tag{33}$$

Taking into account the formula (24), we derive that

$$\langle \mathcal{A}(\boldsymbol{p})\rangle = \mathcal{N}\langle \mathcal{R}_\delta(\boldsymbol{p})\rangle, \tag{34}$$

where

$$\langle \mathcal{R}_\delta(\boldsymbol{p})\rangle = 2\pi|\boldsymbol{p}|\mathcal{R}_\delta^{(0)}\langle\delta(Q)\rangle - |\boldsymbol{p}|\left\langle\frac{1}{Q+i\epsilon}\right\rangle\mathcal{R}_\delta^{(1)} + \mathcal{R}_\delta^{(2)}. \tag{35}$$

Here we have assumed that the amplitudes $\mathcal{R}_\delta^{(0)}$, $\mathcal{R}_\delta^{(1)}$, and $\mathcal{R}_\delta^{(2)}$ are slowly varying functions of their arguments. In addition,

$$\langle\delta(Q)\rangle = \int d^3\boldsymbol{q}\,\delta(Q_{\boldsymbol{q}})f_{\boldsymbol{p}}(\boldsymbol{q}), \tag{36}$$

$$\left\langle\frac{1}{Q+i\epsilon}\right\rangle = \int d^3\boldsymbol{q}\,\frac{f_{\boldsymbol{p}}(\boldsymbol{q})}{Q_{\boldsymbol{q}}+i\epsilon}, \tag{37}$$

and $Q_{\boldsymbol{q}} = E_B + \omega_{\boldsymbol{K}} - \frac{q^2}{2m_e}$. Thus, the momentum profile smears the singularity at $Q=0$ in Eq. (35). Importantly, the resulting probability amplitude (34) accounts coherently for contributions from different electron scattering waves contributing to the wave packet (32). In the following, we will use the amplitude (34) to define the energy distribution of laser-assisted recombination radiation.

Based on Eq. (34), we define the total energy [per the initial electron flux $j_e(\boldsymbol{p})$] that is irradiated due to the interaction of an electron wave packet with a H atom in the presence of a laser field,

$$E(\boldsymbol{p}) = \frac{1}{j_e(\boldsymbol{p})}\int\frac{V d^3\boldsymbol{K}}{(2\pi)^3}\,\omega_{\boldsymbol{K}}|\langle\mathcal{A}(\boldsymbol{p})\rangle|^2. \tag{38}$$

Here we integrate over the density of final radiation states $Vd^3\boldsymbol{K}/(2\pi)^3$. Next, using the relation $|\boldsymbol{K}| = \omega_{\boldsymbol{K}}/c$, we derive that $d^3\boldsymbol{K} = \omega_{\boldsymbol{K}}^2 d\omega_{\boldsymbol{K}} d^2\Omega_{\boldsymbol{K}}/c^3$, where $d^2\Omega_{\boldsymbol{K}}$ is the solid angle of emitted photons. One can also figure out that the initial electron flux is

$$j_e(\boldsymbol{p}) = \frac{|\boldsymbol{p}|}{m_e}\frac{1}{V}. \tag{39}$$

Substituting Eqs. (23), (34), and (39) into (38), we obtain

$$E(\boldsymbol{p}) = \frac{4\alpha}{\pi c^2}\frac{m_e}{|\boldsymbol{p}|}\int d^2\Omega_{\boldsymbol{K}}\int d\omega_{\boldsymbol{K}}\,\omega_{\boldsymbol{K}}^4|\langle\mathcal{R}_\delta(\boldsymbol{p})\rangle|^2. \tag{40}$$

Rewriting this formula as

$$E(\boldsymbol{p}) = \int d^2\Omega_{\boldsymbol{K}}\int d\omega_{\boldsymbol{K}}\frac{d^3E_{\boldsymbol{K}}(\boldsymbol{p})}{d\omega_{\boldsymbol{K}}d^2\Omega_{\boldsymbol{K}}}, \tag{41}$$

we conclude that the triply differential energy distribution (per the initial electron flux) of photons emitted in the solid angle $d^2\Omega_{\boldsymbol{K}}$ and having energy within the interval $(\omega_{\boldsymbol{K}}, \omega_{\boldsymbol{K}}+d\omega_{\boldsymbol{K}})$ is

$$\frac{d^3E_{\boldsymbol{K}}(\boldsymbol{p})}{d\omega_{\boldsymbol{K}}d^2\Omega_{\boldsymbol{K}}} = \frac{4\alpha}{\pi c^2}\frac{m_e}{|\boldsymbol{p}|}\omega_{\boldsymbol{K}}^4|\langle\mathcal{R}_\delta(\boldsymbol{p})\rangle|^2, \tag{42}$$

with $\langle\mathcal{R}_\delta(\boldsymbol{p})\rangle$ given in (35). This is the main result of our theoretical formulation, which will be illustrated numerically in Sec. III. It will be also compared there with the simplified formulation of LARR, as introduced in Ref. [32]. For completeness, we will present the aforementioned formulation below.

C. Simplified formulation of LARR

Following Ref. [32], it is tempting to replace Eq. (14) by

$$\mathcal{A}(\boldsymbol{p}) = 4iA\sqrt{\frac{\pi\omega_{\boldsymbol{K}}}{2\epsilon_0}}\frac{e}{V}\int_0^{T_p}dt\,\frac{\boldsymbol{\varepsilon}_{\boldsymbol{K}}\cdot[\boldsymbol{p}-e\boldsymbol{A}(t)]}{[\kappa^2+\boldsymbol{\pi}^2(t)]^2}e^{iQt+iH(t)}, \tag{43}$$

where we have restricted the time integral to the interval from 0 to T_p. This is equivalent to replacing the function $G(t) = \frac{\boldsymbol{\varepsilon}_{\boldsymbol{K}}\cdot[\boldsymbol{p}-e\boldsymbol{A}(t)]}{[\kappa^2+\boldsymbol{\pi}^2(t)]^2}$ by $G(t)\theta(t)\theta(T_p-t)$, where $\theta(\cdot)$ is the step function. Here the integrand is forcefully set up to zero at times $t=0$ and $t=T_p$, which introduces discontinuity of the integrand at those times. As we will discuss in Sec. III, such an abrupt cutoff of the integration limits will lead to some spurious effects. At this point, we also note that the above formula coincides with Eq. (14) only if $\boldsymbol{\varepsilon}_{\boldsymbol{K}}\cdot\boldsymbol{p}=0$, i.e., when the LARR photons are polarized in the direction perpendicular to the electron's initial momentum. In this case, photons are generated along the propagation direction of the electron, which is the least favorable configuration for LARR. In fact, we will compare both formulations numerically in Sec. III. To proceed, we introduce here $\boldsymbol{\varepsilon}_{\boldsymbol{K}}$ in the most general form given by Eq. (18). Defining

$$\tilde{\mathcal{R}}_j = A\int_0^{T_p}dt\,\frac{\boldsymbol{\varepsilon}_{\boldsymbol{K}j}\cdot[\boldsymbol{p}-e\boldsymbol{A}(t)]}{[\kappa^2+\boldsymbol{\pi}^2(t)]^2}e^{iQt+iH(t)}, \tag{44}$$

along with

$$\tilde{\mathcal{R}}_\delta = \cos\delta\tilde{\mathcal{R}}_1 + i\sin\delta\tilde{\mathcal{R}}_2, \tag{45}$$

we can rewrite Eq. (43) in a more concise form $\mathcal{A}(\boldsymbol{p}) = \mathcal{N}\tilde{\mathcal{R}}_\delta$, with $\mathcal{N}$ defined by Eq. (23). To have a reliable comparison with the results based on the formulation presented in the preceding section, we introduce now the averaging with respect to the initial electron momentum distribution $f_{\boldsymbol{p}}(\boldsymbol{q})$ [Eq. (33)]. Since $\tilde{\mathcal{R}}_\delta$ is a regular function of the electron momentum, such averaging basically gives

$$\langle\mathcal{A}(\boldsymbol{p})\rangle = \mathcal{N}\tilde{\mathcal{R}}_\delta(\boldsymbol{p}). \tag{46}$$

Hence, following derivations from Sec. II B, we find that the energy distribution per the initial electron flux is given by exactly the same formula as (42) except that now $\langle\mathcal{R}_\delta(\boldsymbol{p})\rangle$ is replaced by $\tilde{\mathcal{R}}_\delta(\boldsymbol{p})$. Thus, in Sec. III we will calculate (42) numerically and compare it for both formulations.

D. Electron-wave-packet model

Here we specify the profile of the initial electron wave packet $f_{\boldsymbol{p}}(\boldsymbol{q})$ satisfying the condition (31), which will be used in our numerical analysis. In order to perform integrals over all intermediate momenta, like the one in Eq. (33), it is useful to define the cylindrical coordinates with respect to the direction of the central momentum of the electron wave packet, $\boldsymbol{n}_{\boldsymbol{p}} = \boldsymbol{p}/|\boldsymbol{p}|$. Specifically, we use the longitudinal and the transverse components of electron momenta, $q_\parallel = \boldsymbol{q}\cdot\boldsymbol{n}_{\boldsymbol{p}}$ and $\boldsymbol{q}_\perp = \boldsymbol{q} - q_\parallel\boldsymbol{n}_{\boldsymbol{p}}$, respectively. For a well-collimated electron beam, we assume that

$$f_{\boldsymbol{p}}(\boldsymbol{q}) \approx \frac{1}{\pi}\frac{\Delta|\boldsymbol{p}|}{(q_\parallel-|\boldsymbol{p}|)^2+(\Delta|\boldsymbol{p}|)^2}\delta^{(2)}(\boldsymbol{q}_\perp), \tag{47}$$

where we neglect the spread of the electron wave packet in the direction perpendicular to $\boldsymbol{p}$. The contributing longitudinal momentum components, on the other hand, are distributed according to the Lorentzian function which is peaked at $|\boldsymbol{p}|$ and has the half-width at half maximum (HWHM) equal to $\Delta|\boldsymbol{p}|$. It also holds that

$$\lim_{\Delta|\boldsymbol{p}|\to 0} \frac{1}{\pi} \frac{\Delta|\boldsymbol{p}|}{(q_\parallel - |\boldsymbol{p}|)^2 + (\Delta|\boldsymbol{p}|)^2} = \delta^{(1)}(q_\parallel - |\boldsymbol{p}|). \tag{48}$$

With such a model of the wave-packet profile (47), we can calculate now the averages given by Eqs. (36) and (37). Hence, we obtain

$$\langle \delta(Q) \rangle = \frac{m_e}{\pi q_0} \frac{\Delta|\boldsymbol{p}|}{(q_0 - |\boldsymbol{p}|)^2 + (\Delta|\boldsymbol{p}|)^2} \tag{49}$$

and

$$\left\langle \frac{1}{Q + i\epsilon} \right\rangle = \frac{2m_e}{q_0^2 - \boldsymbol{p}^2 - 2i|\boldsymbol{p}|\Delta|\boldsymbol{p}|} - 2i\pi \langle \delta(Q) \rangle, \tag{50}$$

where $q_0 = \sqrt{2m_e(E_B + \omega_K)}$ is the magnitude of the initial electron momentum which results in the field-free peak. In deriving Eq. (50) we used the Sokhotski-Plemelj formula (25). Note also that it was derived to the leading order in $\Delta|\boldsymbol{p}|$. Finally, combining it with $\langle \frac{1}{Q+i\epsilon} \rangle = \langle \mathcal{P}(\frac{1}{Q}) \rangle - i\pi \langle \delta(Q) \rangle$, we obtain that, to the leading order in $\Delta|\boldsymbol{p}|$, the following holds:

$$\left\langle \mathcal{P}\left(\frac{1}{Q}\right) \right\rangle = \frac{2m_e}{q_0^2 - \boldsymbol{p}^2 - 2i|\boldsymbol{p}|\Delta|\boldsymbol{p}|} - i\pi \langle \delta(Q) \rangle. \tag{51}$$

It follows from these equations that at $|\boldsymbol{p}| = q_0$, i.e., when $Q = 0$, we have $\langle \delta(Q) \rangle = O(\frac{1}{\Delta|\boldsymbol{p}|})$ and $\langle \mathcal{P}(\frac{1}{Q}) \rangle = O((\frac{1}{\Delta|\boldsymbol{p}|})^0)$. Furthermore, these formulas allow us to calculate $\langle \mathcal{R}_\delta(\boldsymbol{p}) \rangle$ according to Eq. (35) and hence the energy distribution defined by Eq. (42). This will be done for a model of the laser field introduced below.

E. Laser-field model

In our numerical illustrations, we will use a linearly polarized laser field that is described by the vector potential $\boldsymbol{A}(t) = A(t)\boldsymbol{\varepsilon}$ such that

$$A(t) = \begin{cases} A_0 \sin^{2M}(\frac{\omega t}{2N_{\rm osc}}) \sin(\omega t + \chi) & \text{for } 0 \leqslant t \leqslant T_p \\ 0 & \text{otherwise.} \end{cases} \tag{52}$$

It represents a train of identical $N_{\rm rep}$ laser pulses where each of them lasts for $\tau_p = 2\pi N_{\rm osc}/\omega$. Since they have minimal delay to guarantee their temporal separation, the time duration of the train equals $T_p = N_{\rm rep}\tau_p$. Here ω is the carrier frequency, $N_{\rm osc}$ defines the number of cycles within a pulse, χ is the carrier-envelope phase (CEP), and the parameter M is used to shape the envelope of a single pulse. We define the constant A_0 such that the corresponding electric field $\boldsymbol{\mathcal{E}}(t) = \mathcal{E}(t)\boldsymbol{\varepsilon}$, where $\mathcal{E}(t) = -dA(t)/dt$, satisfies the condition

$$\max_t |\mathcal{E}(t)| = \eta \mathcal{E}_0. \tag{53}$$

In principle, η is an arbitrary constant. This means that the maximum intensity equals

$$I_{\rm max} = \epsilon_0 c \eta^2 \mathcal{E}_0^2 = \eta^2 I_0. \tag{54}$$

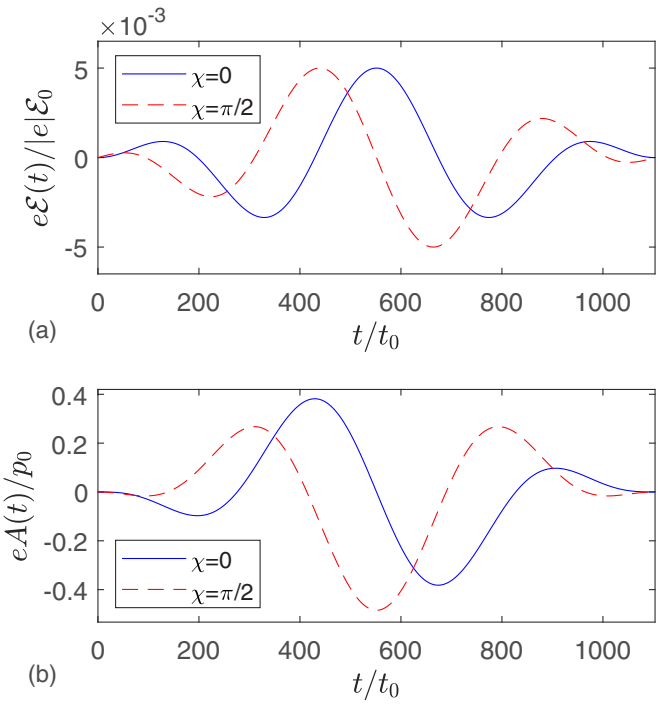

FIG. 1. (a) Electric field $\mathcal{E}(t)$ and (b) vector potential $A(t)$ representing a two-cycle ($N_{\rm osc} = 2$), sine-squared ($M = 1$) laser pulse (52) ($N_{\rm rep} = 1$) such that $\lambda = 4000$ nm, $\eta = 0.005$, and the CEP is either $\chi = 0$ or $\pi/2$, as shown in the legend.

As an example, in Fig. 1 we plot the time dependence of the electric field $\mathcal{E}(t)$ and the vector potential $A(t)$ for a two-cycle laser pulse ($N_{\rm rep} = 1$ and $N_{\rm osc} = 2$) with the wavelength $\lambda = 2\pi c/\omega = 4000$ nm (hence $\omega = 0.31$ eV) and the sine-squared envelope ($M = 1$). In addition, $\chi = 0$ (solid line) or $\chi = \pi/2$ (dashed line), whereas the peak intensity of the pulse is determined by the parameter $\eta = 0.005$. As one can see from Fig. 1, the vector potential satisfies the condition $A(0) = A(T_p) = 0$ (here $T_p = \tau_p$), which follows from a more fundamental requirement that for the laser field, $\int_{-\infty}^{\infty} dt\, \mathcal{E}(t) = 0$. The same holds true for our train of identical pulses (52), as $A(\ell\tau_p) = 0$ for $\ell = 0, 1, \ldots, N_{\rm rep}$. At this point, it is worth mentioning that the same laser-field parameters have been used in our works on strong-field ionization of H^- [42,43]. In those papers, we showed that the SFA gives nearly the same results as numerical integration of the time-dependent Schrödinger equation with the electron-atom interaction being modeled by the short-range Yukawa potential. This indicates that the current parameters are also justified for the SFA-based description of LARR presented in this paper. For such models of the laser field, we present next the directional energy distributions of emitted radiation.

III. NUMERICAL ILLUSTRATIONS

A. Energy distributions of laser-assisted recombination radiation

Figure 2 shows the energy distributions of emitted radiation resulting from the interaction of a coherent electron wave packet with a hydrogen atom assisted by the laser pulse;

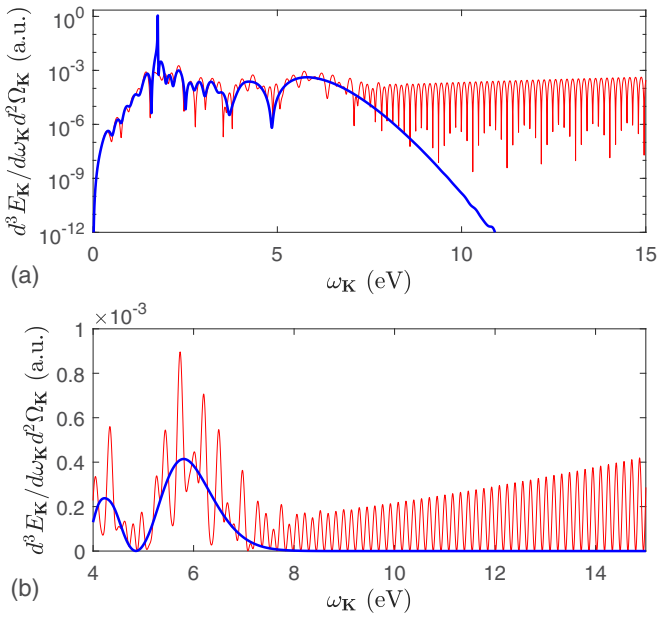

FIG. 2. Energy spectra of radiation emitted by an electron evolving in a laser pulse and being captured by a hydrogen atom. The laser pulse is plotted in Fig. 1 for $\chi = 0$. The electron is represented by the wave packet centered at momentum $\boldsymbol{p}$ such that $E_{\boldsymbol{p}} = \frac{p^2}{2m_e} = 1\,\mathrm{eV}$. The momentum profile of the wave packet (47) is well collimated, with the longitudinal spread $\Delta|\boldsymbol{p}| = m_e/\zeta|\boldsymbol{p}|\tau_p$, where $\zeta = 10^4$. The thick blue curve corresponds to Eq. (42), whereas the thin red curve follows from the simplified LARR theory, as introduced in Sec. II C. (a) Plot of the data in logarithmic scale and (b) the high-energy portion of the spectra (which does not contain the field-free peak) plotted in linear scale.

the latter was represented in Fig. 1 for $\chi = 0$. We assume that the central momentum of the electron wave packet (47) corresponds to its initial kinetic energy $E_{\boldsymbol{p}} = \frac{p^2}{2m_e} = 1\,\mathrm{eV}$. In order to estimate the HWHM in the electron momentum distribution (47), we note that the following relation holds: $\Delta E_{\boldsymbol{p}} = \frac{|\boldsymbol{p}|}{m_e}\Delta|\boldsymbol{p}|$. We ensure that the electron wave packet does not spread much during the interaction with the laser pulse, i.e., over time τ_p. This is satisfied provided $\Delta E_{\boldsymbol{p}}\tau_p \ll 1$. We can choose $\zeta \gg 1$ such that $\Delta E_{\boldsymbol{p}}\tau_p = \zeta^{-1}$. Hence, the HWHM of the momentum distribution (47) equals $\Delta|\boldsymbol{p}| = m_e/\zeta|\boldsymbol{p}|\tau_p$. For numerical purposes we take the parameter $\zeta = 10^4$. Moreover, we choose the geometry such that $\boldsymbol{n}_{\boldsymbol{p}} = \boldsymbol{e}_x$ and $\boldsymbol{n}_{\boldsymbol{K}} = c\boldsymbol{K}/\omega_{\boldsymbol{K}} = \boldsymbol{e}_z$. This means that $\boldsymbol{p}\cdot\boldsymbol{K} = 0$, which makes for the most efficient generation of the laser-assisted recombination radiation. For the given geometry, we plot the energy distribution of radiation that is calculated either according to Eq. (42) (thick blue line) or using a simplified theorem based on Eq. (46) (thin red line). The results are presented in logarithmic scale in Fig. 2(a) and their enlarged portions are shown in linear scale in Fig. 2(b). Note that, for the current parameters, the generated radiation is in the infrared and near-ultraviolet parts of the spectrum. The reason is that we deal with a rather low-energy electron beam, so the energy transfer is also limited. Importantly, we can see in Fig. 2(a) that the simplified formulation of LARR leads to an unphysical plateau in the high-energy portion of the distribution. This tail is an artifact originating from the Gibbs effect, which occurs in the band-limited Fourier analysis [38,39]. Also the oscillations, which are shown clearly in Fig. 2(b), follow from the Gibbs phenomenon. They are not present in the LARR energy spectrum calculated from Eq. (42). Another pronounced difference is that, while the energy distribution (42) exhibits a characteristic peak at the field-free energy (30), the simplified theory presented in Sec. II C does not predict that. Despite these differences, the overall behaviors of both distributions seem to be similar.

At this point, we note that the focus of this paper is on radiative recombination assisted by laser pulses which are much shorter in duration than the electron wave packet. The latter is represented by $1/\Delta E_{\boldsymbol{p}} = m_e/|\boldsymbol{p}|\Delta|\boldsymbol{p}| = \zeta\tau_p$ and indeed is much smaller than T_p. In this case, the radiation spectrum comprises of a very narrow peak and a plateau. As it follows from Eq. (48), the width of the peak is inversely proportional to the time duration of the electron wave packet. This means that the field-modified contribution to recombination spectrum [Eq. (27)] is defined for $\omega_{\boldsymbol{K}}$ for which the equality $Q = 0$ is closely satisfied. The field-induced contribution [Eq. (28)], on one hand, is defined for such an $\omega_{\boldsymbol{K}}$ for which $Q \neq 0$, which is dictated by the principal value $\mathcal{P}(1/Q)$. On the other hand, Eq. (28) also contains $R_\delta^{(2)}$, which is a continuous function of Q. This in principle should lead to interference between field-modified and field-induced contributions in the spectral distribution of emitted radiation. It follows from Eqs. (49) and (51), however, that the interference term is negligible (as compared to the laser-modified one) as long as we deal with long electron wave packets. Thus, we attribute the peak in the spectrum to the field-modified process and the plateau to the field-induced process. The two distinct patterns will also be seen in spectrograms presented in Sec. III C.

In Fig. 3 we present the results for $E_{\boldsymbol{p}} = 30\,\mathrm{eV}$, with the remaining parameters the same as in Fig. 2. Naturally enough, the radiation spectrum shown in Fig. 3(a) extends towards larger energies, reaching the extreme ultraviolet portion of the spectrum. We still observe artificial wiggles in the distribution marked by the red curve, which are followed by the high-energy oscillations extending far beyond the actual range of emitted radiation. The latter can be explained qualitatively with the help of Fig. 3(b), where we plot

$$\omega_{\boldsymbol{K}}(t) = \frac{1}{2m_e}[\boldsymbol{p} - e\boldsymbol{A}(t)]^2 - E_B. \tag{55}$$

This quantity appears in the classical analysis of LARR [24,30,31], where it represents the energy emitted by an electron of momentum $\boldsymbol{p}$ that evolves in a laser pulse and is captured at time t by the atom (see, e.g., Ref. [24]). The range of (55) is marked with the black vertical lines in both Figs. 3(a) and 3(b). Since we deal with an electron wave packet instead, where $\boldsymbol{p}$ represents its central momentum, those black lines do not exactly match the end points of the radiation spectrum, as it has been demonstrated in [24] for a bichromatic laser field. Nevertheless, they clearly mark the cutoff of the plateau in the LARR spectrum. In Fig. 3(a) one can also distinguish regions with regular and irregular oscillations, being separated by the green vertical lines. They match very well the corresponding regions in Fig. 3(b). Here we distinguish the regions where the radiation of a given energy can

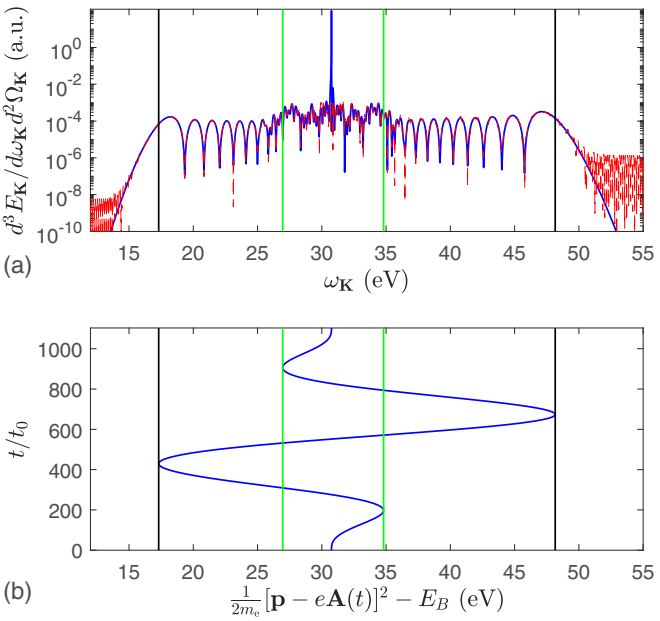

FIG. 3. (a) Energy spectra of emitted radiation for the same parameters as in Fig. 2, except that now $E_p = 30\,\text{eV}$. The vertical black lines mark the irradiated energy cutoffs. In addition, the vertical green lines mark the borders between the regions of regular and erratic oscillations. Each of them follows from the analysis of (55), whose time dependence is plotted in (b).

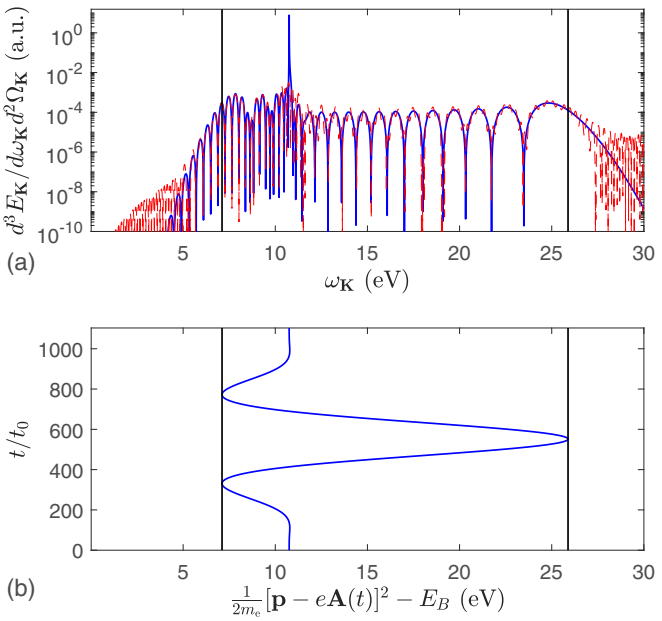

FIG. 4. Same as in Fig. 3 for the laser pulse given by Eq. (52), except that here $M = 2$, $\chi = \pi/2$, and $E_p = 10\,\text{eV}$.

be emitted either at two different times or more frequently. For the former, the distribution exhibits very regular oscillations as the result of interference of only two LARR probability amplitudes. The interference of four probability amplitudes at energies corresponding to the central region in Fig. 3(b) causes a rather erratic behavior of the radiation spectrum. The same is observed for a different pulse model, as presented in Fig. 4. In either case, the simplified theory of LARR shows additional wiggles that we can see clearly in linear scale, for instance, in Fig. 5 where the portions of the spectra from Fig. 3 are presented. In addition, as we have checked in this case, the nonphysical tail acquires a maximum at roughly 5 keV. This maximum is comparable in magnitude to the plateau present in Fig. 3. Still, we would like to caution that it is an artifact that follows from restricting the limits of the time integral in the probability amplitude of LARR. Another manifestation of the Gibbs phenomenon relates to spectrograms and it will be presented in Sec. III C.

In closing this section, let us stress that qualitatively the same results are obtained for other laser-field parameters, including more common wavelengths in the midinfrared range. In this case, however, in order to observe effects similar to those presented in our paper one has to increase the amplitude of the laser field. Then the corresponding energy distributions of emitted radiation have similar structure except that the interference pattern which they exhibit is less pronounced. We also believe that the presented SFA-based LARR theory is justified for higher intensities of a Ti:sapphire laser field and positively charged ions such as He^+, with much higher binding energies. In this case, however, one has to investigate the influence of the long-range Coulomb potential on the resulting distributions of emitted radiation. This can be done, for instance, by replacing the Volkov solution in the initial electron state by the Coulomb-Volkov solution.

B. Frequency combs

Another important aspect to investigate is the effect of a train of pulses on the LARR energy spectrum. For this purpose, we consider the recombination assisted by a repetition of two ($N_{\text{rep}} = 2$) and three ($N_{\text{rep}} = 3$) laser pulses

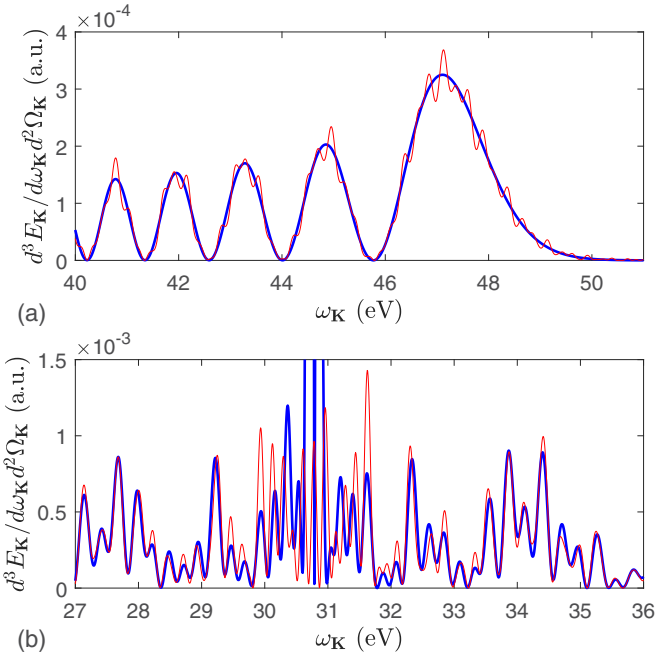

FIG. 5. Enlarged portions of the spectra shown in Fig. 3 in linear scale.

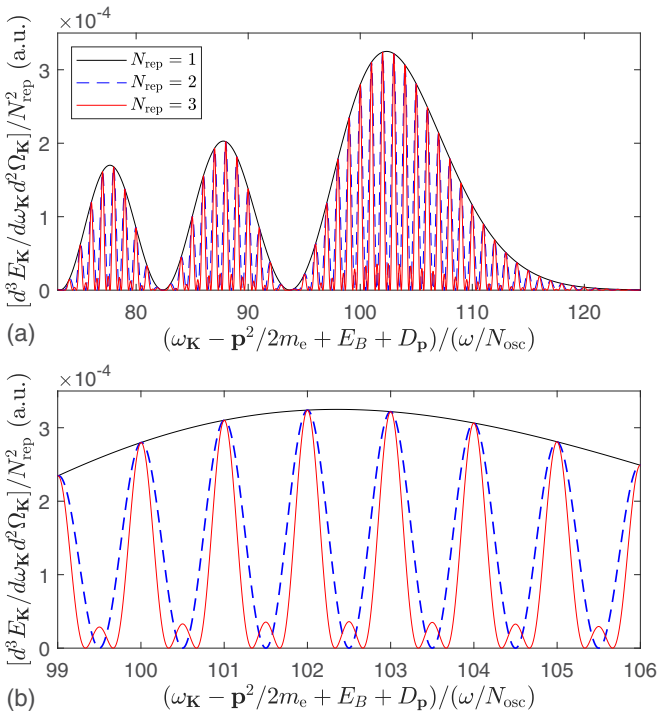

FIG. 6. Energy distributions of laser-assisted recombination radiation (42) emitted in the presence of an isolated pulse ($N_{\rm rep}=1$) that is represented in Fig. 1 for $\chi=0$ and a train of two ($N_{\rm rep}=2$) or three ($N_{\rm rep}=3$) such pulses. The remaining parameters are the same as in Fig. 3. The spectra have been divided by $N_{\rm rep}^2$.

presented in Fig. 1 for $\chi=0$. In both cases we observe a LARR energy spectrum similar to that presented in Figs. 3 and 5, with an extended plateau followed by sharp cutoffs. According to our analysis above, the latter should occur at the same energies as for the pulse, which has been confirmed by our numerical results. There is also the δ-like peak embedded in the spectrum. To see the difference, in Fig. 6 we plot the enlarged portions of the energy distributions (42) divided by $N_{\rm rep}^2$. Because of the scaling, the results for a pulse form the envelope for other spectra, here marked with the blue dashed ($N_{\rm rep}=2$) and the red solid ($N_{\rm rep}=3$) lines. As one can see, if the recombination is assisted by a train of pulses, the energy distributions of emitted radiation exhibit comblike structures with the characteristic $N_{\rm rep}^2$ scaling. At the same time, the total energy of emitted radiation is increased by a factor $N_{\rm rep}$ because each linewidth is narrowed by the factor $1/N_{\rm rep}$. The qualitative explanation of this effect can be based on derivations presented in Sec. IV. Namely, we can relate these derivations to Eq. (16), however, neglecting the δ peak. In doing so, we represent the field-induced contribution of the probability amplitude of recombination assisted by a train of $N_{\rm rep}$ pulses as

$$\mathcal{A}_{N_{\rm rep}}(\boldsymbol{p}) = e^{(i/2)(Q+D_{\boldsymbol{p}})(N_{\rm rep}-1)\tau_p}\mathcal{A}_1(\boldsymbol{p}) \times \frac{\sin\left[\frac{1}{2}(Q+D_{\boldsymbol{p}})N_{\rm rep}\tau_p\right]}{\sin\left[\frac{1}{2}(Q+D_{\boldsymbol{p}})\tau_p\right]}, \tag{56}$$

where we have adapted Eq. (C9) to our current situation. Specifically, $\mathcal{A}_1(\boldsymbol{p})$ stands here for the probability amplitude of recombination assisted by a pulse, Q is given by Eq. (10), and

$$D_{\boldsymbol{p}} = \frac{1}{\tau_p}H(\tau_p), \tag{57}$$

with $H(t)$ defined by Eq. (11). We conclude from Eq. (56) that the probability amplitude $\mathcal{A}_{N_{\rm rep}}$ takes the maximum values when

$$\left(\omega_{\boldsymbol{K}} - \frac{\boldsymbol{p}^2}{2m_e} + E_B + D_{\boldsymbol{p}}\right)\frac{N_{\rm osc}}{\omega} = N, \quad N\in\mathbb{Z}, \tag{58}$$

where we have written explicitly the value of Q and substituted $\tau_p=\frac{2\pi}{\omega}N_{\rm osc}$. At those energies $\omega_{\boldsymbol{K}}$, the interference factor given by the sine functions equals $N_{\rm rep}$. Thus, the respective probability distributions will be enhanced by a factor of $N_{\rm rep}^2$ compared to the results for a single pulse. Note also that this enhancement originates from constructive interference of the probability amplitudes of recombination assisted by each pulse from the train. Another characteristic property of the LARR spectra is that for $N_{\rm rep}\geqslant 2$ there appear also $N_{\rm rep}-2$ secondary maxima, as shown in Fig. 6. As we have also checked, with increasing $N_{\rm rep}$ the major peaks become more narrow. Thus, the spectrum of laser-assisted recombination radiation becomes similar to a Dirac comb.

We have demonstrated that, due to the electron-atom recombination in the presence of a pulse train, the frequency combs can be generated. Specifically, for the data presented in Fig. 6 they fall into the extreme ultraviolet regime. In addition, by increasing the energy of the initial electron beam, we can extend their range even more. We have therefore a tool for producing the radiation combs whose energy can be tuned by the electron beam. Similarly, it can be done in laser-induced Compton or Thomson scattering, as proposed, for instance, in Refs. [44,45].

C. Energy distribution spectrograms

Our aim now is to define the spectrogram $S(t,\omega_{\boldsymbol{K}})$ of a signal $\mathcal{A}(\omega)$, where the latter is specified for $\omega_1\leqslant\omega\leqslant\omega_2$. For this purpose, we truncate the signal such that it takes zero values at the boundaries ω_1 and ω_2. The reason is that the spectrogram is calculated using the Fourier transform. In this case, to avoid the Gibbs phenomenon, the integrand has to be continuous and takes the same values at the boundaries. Therefore, we define the truncated signal

$$\mathcal{A}_T(\omega) = \mathcal{A}(\omega)f_T\left(\frac{\omega-\omega_1}{\omega_2-\omega_1}, \xi_T(\omega_2-\omega_1)\right), \tag{59}$$

where ξ_T is a small parameter and

$$f_T(x,\Delta x) = \begin{cases} 0 & \text{for } x\leqslant 0 \\ \sin^2(\frac{\pi x}{2\Delta x}) & \text{for } 0<x<\Delta x \\ 1 & \text{for } \Delta x\leqslant x\leqslant 1-\Delta x \\ \sin^2(\frac{\pi(1-x)}{2\Delta x}) & \text{for } 1-\Delta x<x<1 \\ 0 & \text{for } x\geqslant 1. \end{cases} \tag{60}$$

Next we define the short-time Fourier transform of the truncated signal [46]

$$\mathcal{A}_{\rm ST}(t,\omega_{\boldsymbol{K}}) = \int_{\omega_1}^{\omega_2} d\omega\, \mathcal{A}_T(\omega)W(\omega-\omega_{\boldsymbol{K}}, \xi_W(\omega_2-\omega_1))e^{-i\omega t}, \tag{61}$$

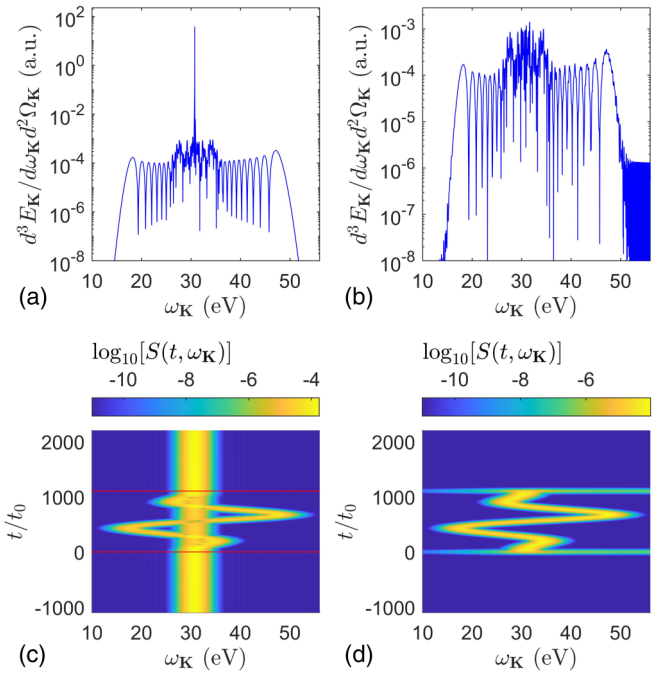

FIG. 7. (a) and (b) Energy distributions of emitted laser-assisted recombination radiation that have been presented in Fig. 3. The spectra were calculated (a) within the complete theory (Sec. II B) and (b) for its simplified version (Sec. II C). (c) and (d) Their corresponding spectrograms were calculated using the Gaussian window (62) and the cutoff function (60), with the parameters $\xi_T = 0.1$, $\xi_W = 0.03$, $\omega_1 = 1\,\text{eV}$, and $\omega_2 = 65\,\text{eV}$. In (c) the red horizontal lines mark the beginning and the end of the laser pulse.

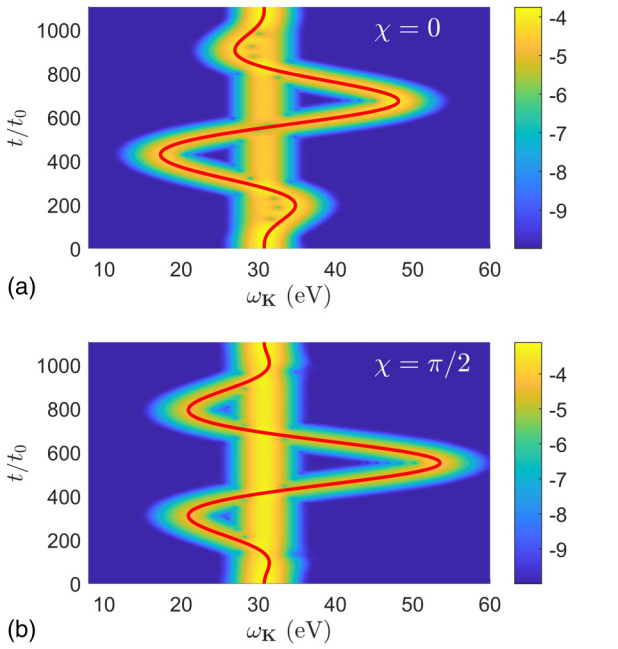

FIG. 8. Spectrograms of the energy distribution (42) calculated for laser pulses represented in Fig. 1 for (a) $\chi = 0$ and (b) $\chi = \pi/2$. The remaining parameters are the same as in Fig. 7. Red lines represent the time dependence of $\omega_{\boldsymbol{K}}(t)$ given by Eq. (55).

where ξ_W is a parameter determining the width of the window function $W(x, \Delta x)$. For our purpose, we assume the Gaussian window

$$W(x, \Delta x) = \frac{e^{-(x/\Delta x)^2}}{\sqrt{\pi}\,\Delta x}, \tag{62}$$

which satisfies the condition

$$\int_{-\infty}^{\infty} dx\, W(x, \Delta x) = 1. \tag{63}$$

Note that if the window is a low-pass function, then evaluating the integral (61) can be understood as sending the signal through a bandpass filter $W(\omega - \omega_{\boldsymbol{K}}, \xi_W(\omega_2 - \omega_1))$ centered at the output frequency $\omega_{\boldsymbol{K}}$. Thus, it can be thought of as the temporal fluctuations of the signal spectrum near the frequency $\omega_{\boldsymbol{K}}$ [46]. With this in mind, we define the spectrogram as

$$S(t, \omega_{\boldsymbol{K}}) = |\mathcal{A}_{\text{ST}}(t, \omega_{\boldsymbol{K}})|^2. \tag{64}$$

For our purpose, it is good to realize that if the truncated signal is peaked at ω_0, namely, $\mathcal{A}_T(\omega) \approx \delta(\omega - \omega_0)$, then $S(t, \omega_{\boldsymbol{K}}) \approx |W(\omega_0 - \omega_{\boldsymbol{K}}, \xi_W(\omega_2 - \omega_1))|^2$. In other words, the spectrogram represents the window function squared which is shifted by ω_0 and, most importantly, it does not depend on time. This will be helpful to interpret our results.

In Fig. 7 we show the energy spectra [Figs. 7(a) and 7(b)] and their corresponding spectrograms [Figs. 7(c) and 7(d)] calculated according to the above prescription. For the cutoff function and for the window we have used Eqs. (60) and (62) with $\xi_T = 0.1$, $\xi_W = 0.03$, $\omega_1 = 1\,\text{eV}$, and $\omega_2 = 65\,\text{eV}$. Note that these are the same energy spectra as presented in Fig. 3. Namely, the results in Figs. 7(a) and 7(c) have been calculated according to the complete theory presented in Sec. II B and the results in Figs. 7(b) and 7(d) according to the simplified theory from Sec. II C. We see that there are two distinct patterns in the spectrogram in Fig. 7(c). The straight vertical line at roughly 30 eV corresponds to the field-free peak in the spectrum, which agrees with our analysis of properties of the spectrogram. Obviously, this line extends for times $t < 0$ and $t > \tau_p$, as recombination happens also in the absence of the laser pulse. On top of that line, there is the zigzag pattern that lasts over the entire duration of the pulse (the latter being marked by two horizontal lines). This zigzag pattern shows up also in the spectrogram in Fig. 7(d). What is missing there, however, is the contribution from the field-free process. Instead, two unphysical lines at the pulse turning on and off times appear as evidence of the Gibbs effect, discussed earlier in relation to Eq. (43). Having worked out the concept of the spectrogram, we demonstrate in Sec. III D that it can be efficiently used in metrology of laser fields.

D. LARR-based laser-field metrology

The temporal characterization of a laser field is essential in studying laser-matter interactions. For this reason, we propose a method of retrieving such complete characterization of the laser field from the spectrum of electron-atom LARR. As we show for both isolated pulses and trains of pulses, the method is practically insensitive to the precise temporal shape of the field, thus proving its great versatility.

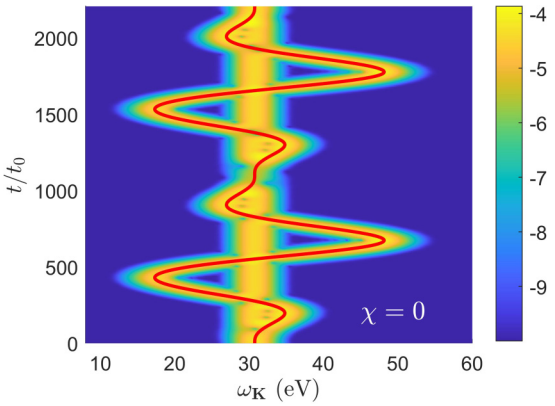

FIG. 9. Same as in Fig. 8 but for the train of two pulses ($N_{\rm rep} = 2$) and the CEP equal to 0.

In Fig. 8 we present the spectrogram of the energy distribution of laser-assisted recombination radiation that is generated in the interaction of an electron with a hydrogen atom and isolated pulses presented in Fig. 1. Figure 8(a) corresponds to the pulse with $\chi = 0$, whereas Fig. 8(b) is for $\chi = \pi/2$. The parameters used for calculations are the same as in Fig. 7. As already discussed in the preceding section, both spectrograms show the pattern which originates from the field-free recombination. It is the zigzag pattern, however, that is most important from the point of view of laser-field reconstruction. Obviously, it varies between both panels depending on the CEP of the pulse. However, in both cases it follows the red line, which represents the energy released during the pulse duration by the recombining electron, i.e., $\omega_{\boldsymbol{K}}(t)$ given by Eq. (55). Since $\omega_{\boldsymbol{K}}(t)$ depends on the vector potential of the laser field, we can conclude that $\boldsymbol{A}(t)$ can be reconstructed from the spectrogram of the energy distributions of laser-assisted recombination radiation [Eq. (64)]. This is provided the binding energy of the target and the momentum distribution of the initial electron wave packet are known.

As we have already mentioned, our approach also can be used for *in situ* characterization of a train of pulses. For illustration, we show in Fig. 9 the spectrogram of the energy spectrum of laser-assisted recombination radiation in the case when the process occurs in the presence of a train of two laser pulses ($N_{\rm rep} = 2$). The remaining parameters are the same as in Fig. 8 with $\chi = 0$. As we see, the spectrogram shows the same properties as for a single pulse. Most importantly, the energy $\omega_{\boldsymbol{K}}(t)$ released by a recombining electron at time t while interacting with the laser field is imprinted in the spectrogram. This is again emphasized by the red solid line, which represents the analytical form of $\omega_{\boldsymbol{K}}(t)$.

IV. SUMMARY

We have presented a comprehensive theoretical description of laser-assisted electron-atom radiative recombination, which incorporates contributions from the laser-field-free process along with the laser-field-modified process. This improves the originally introduced formulation of LARR by Bivona *et al.* [32]. We demonstrated various differences between our comprehensive treatment of LARR and the one published in [32]. This includes unphysical oscillations and a high-energy tail in the spectrum of laser-assisted recombination radiation when calculated using the simplified theory. It also appears there as an unphysical pattern in spectrograms of emitted radiation. As we have shown, those features originate from an artificial cutoff of the range of time integral defining the probability amplitude of LARR and are related to the Gibbs effect.

We studied the electron-atom recombination assisted by an isolated laser pulse and a train of pulses. In both cases, the spectrum of emitted radiation looks similar. Namely, it consists of a δ-like spectrum embedded in the continuum, the extent of which can be estimated from the classical argument presented in Sec. III A. As compared to a single pulse, the energy spectrum of laser-assisted recombination radiation emitted in the presence of a pulse train exhibits an additional structure. More specifically, we observe the frequency combs with the major maxima scaling as $N_{\rm rep}^2$, where $N_{\rm rep}$ is the number of pulses in a train. Such scaling is a signature of coherent enhancement. As it follows from our derivations, it can be attributed to constructive interference of probability amplitudes describing recombination in the presence of each pulse from the train. Also, with increasing $N_{\rm rep}$, the pattern starts to resemble the Dirac comb. It is particularly interesting as our predictions take into account the momentum spread of the initial electron beam. Despite such spread, we still observed very clear comb structures. Moreover, by changing the initial electron beam energy we can in principle generate combs in the broad range of the electromagnetic spectrum. All of these have potential use in various applications in spectroscopy and metrology.

A separate problem is that the experimental observation of LARR is limited. In fact, in neither of the experiments [8–12] was the mechanism of LARR described in our paper directly realized. We believe that performing such an experiment, involving three-body collisions between the laser beam and beams of electrons and atoms (or ions), is a very demanding task. Note that a similar level of difficulty concerns, for instance, the laser-assisted electron diffraction experiments by Kanya *et al.* [47–49]. This suggests that the current mechanism of LARR can in principle be realized in laboratory by experimental groups studying laser-assisted scattering processes. For this to happen, the available experimental setups have to be equipped with radiation detectors.

We showed in the paper that the laser-assisted recombination radiation allows for *in situ* measurement of the laser field. Namely, the vector potential describing the laser field can be fully reconstructed from the spectrogram of the emitted radiation. As long as we consider the electron-atom LARR, the technique is versatile and can be used, in principle, in the broad range of the electromagnetic spectrum. As we have checked, it can also track the CEP variations and is independent of the particular shape of the laser field. Thereby, it can be successfully used in the diagnostics of both isolated pulses and pulse trains.

In closing, we note that our analysis considers the recombination by a short-range atomic potential. In this case, the influence of the Coulomb tail does not blur the effect of the laser field on the LARR spectra. While we expect that the main features of the spectra (such as the appearance

of frequency combs) will be still visible in the presence of the Coulomb interaction, they will surely be modified. The same concerns the proposed LARR-based laser diagnostic method, which works very well for electron-atom radiative recombination but still has to be verified for the electron-ion process.

ACKNOWLEDGMENTS

This work was supported by the National Science Centre (Poland) under Grants No. 2018/30/Q/ST2/00236 (D.K. and K.K.) and No. 2018/31/B/ST2/01251 (J.Z.K.), by the National Natural Science Foundation of China under Grants No. 11961131008 and No. 11725416, and by the National Key R&D Program of China under Grant No. 2018YFA0306302 (L.-Y.P.).

APPENDIX A: BOCA-FLORESCU TRANSFORMATION

We consider the regularized integral

$$I(\epsilon)=\int_{-\infty}^{\infty}dt\,\frac{e^{iQt+iH(t)-\epsilon|t|}}{[\kappa^2+\boldsymbol{\pi}^2(t)]^2}, \tag{A1}$$

where $\epsilon>0$ guarantees its absolute convergence. Dividing this integral into two intervals $(-\infty,0]$ and $[0,+\infty)$ and integrating by parts each of the corresponding integrals, we arrive at

$$\begin{aligned}I(\epsilon)=&\frac{e^{iH(0)}}{[\kappa^2+\boldsymbol{\pi}^2(0)]^2}\left(\frac{1}{i(Q-i\epsilon)}-\frac{1}{i(Q+i\epsilon)}\right)\\&-\frac{1}{i(Q-i\epsilon)}\int_{-\infty}^{0}dt\,e^{i(Q-i\epsilon)t}\left(\frac{e^{iH(t)}}{[\kappa^2+\boldsymbol{\pi}^2(t)]^2}\right)'\\&-\frac{1}{i(Q+i\epsilon)}\int_{0}^{\infty}dt\,e^{i(Q+i\epsilon)t}\left(\frac{e^{iH(t)}}{[\kappa^2+\boldsymbol{\pi}^2(t)]^2}\right)',\end{aligned} \tag{A2}$$

where the prime stands for derivative with respect to t. Returning to the definitions (9) and (11), we have

$$H(0)=1,\quad \boldsymbol{\pi}(0)\equiv\boldsymbol{\pi}_0=\boldsymbol{p}-\boldsymbol{K}. \tag{A3}$$

In addition, we introduce the function

$$F(t)=h(t)+4i\frac{e\boldsymbol{\mathcal{E}}(t)\cdot\boldsymbol{\pi}(t)}{\kappa^2+\boldsymbol{\pi}^2(t)}, \tag{A4}$$

with $h(t)$ implicitly defined in Eq. (11). Here $\boldsymbol{\mathcal{E}}(t)=-d\boldsymbol{A}(t)/dt$ is the electric component defining the laser field. Since

$$\left(\frac{e^{iH(t)}}{[\kappa^2+\boldsymbol{\pi}^2(t)]^2}\right)'=\frac{iF(t)}{[\kappa^2+\boldsymbol{\pi}^2(t)]^2}\,e^{iH(t)} \tag{A5}$$

is zero except for the interval $t\in[0,T_p]$, Eq. (A2) takes the form

$$\begin{aligned}I(\epsilon)=&\frac{1}{\left(\kappa^2+\boldsymbol{\pi}_0^2\right)^2}\frac{2\epsilon}{Q^2+\epsilon^2}\\&-\frac{1}{Q+i\epsilon}\int_0^{T_p}dt\,\frac{F(t)}{[\kappa^2+\boldsymbol{\pi}^2(t)]^2}e^{i(Q+i\epsilon)t+iH(t)}.\end{aligned} \tag{A6}$$

In light of Eq. (15), we are interested in the limit of the above expression when $\epsilon\to0$. Using the model of the Dirac δ function

$$\delta(Q)=\lim_{\epsilon\to0}\frac{1}{\pi}\frac{\epsilon}{Q^2+\epsilon^2}, \tag{A7}$$

we obtain, from Eq. (A6),

$$\begin{aligned}\lim_{\epsilon\to0}I(\epsilon)=&\int_{-\infty}^{\infty}dt\,\frac{e^{iQt+iH(t)}}{[\kappa^2+\boldsymbol{\pi}^2(t)]^2}=2\pi\delta(Q)\frac{1}{\left(\kappa^2+\boldsymbol{\pi}_0^2\right)^2}\\&-\frac{1}{Q+i\epsilon}\int_0^{T_p}dt\,\frac{F(t)}{[\kappa^2+\boldsymbol{\pi}^2(t)]^2}e^{iQt+iH(t)},\end{aligned} \tag{A8}$$

which is the foundation of our derivations in Sec. II A. Note that we still keep ϵ in the term $1/(Q+i\epsilon)$, as it defines the prescription of how to handle the singularity at $Q=0$.

APPENDIX B: FIELD-FREE RECOMBINATION

The probability amplitude of recombination of an electron carrying the momentum $\boldsymbol{p}$ by a short-range potential $V(\boldsymbol{r})$ is given by Eq. (4), where the electron scattering state $\psi_{\boldsymbol{p}}^{(+)}(\boldsymbol{r},t)$ is a plane wave

$$\psi_{\boldsymbol{p}}^{(+)}(\boldsymbol{r},t)=\frac{1}{\sqrt{V}}\exp\left(-i\frac{\boldsymbol{p}^2}{2m_{\rm e}}t+i\boldsymbol{p}\cdot\boldsymbol{r}\right). \tag{B1}$$

Similar to Eq. (6), the above wave function is normalized in the volume V. Substituting this formula into Eq. (4) along with Eq. (7), we obtain that, for the field-free process,

$$\mathcal{A}_{\rm FF}=\frac{e}{V}\sqrt{\frac{\omega_{\boldsymbol{K}}}{2\epsilon_0}}\,\tilde{\Phi}_B(\boldsymbol{\pi}_0)\int_{-\infty}^{\infty}dt\,e^{i(E_B+\omega_{\boldsymbol{K}}-\boldsymbol{p}^2/2m_{\rm e})t}, \tag{B2}$$

where $\boldsymbol{\pi}_0$ was defined in Eq. (A3) and $\tilde{\Phi}_B$ for a H^- ion considered in this paper was defined by Eq. (13). Substituting here Eq. (13) and performing the remaining time integral, which gives the Dirac δ function, we conclude that

$$\mathcal{A}_{\rm FF}=8iA\sqrt{\frac{\pi\omega_{\boldsymbol{K}}}{2\epsilon_0}}\frac{\pi e}{V}\frac{\boldsymbol{\varepsilon}_{\boldsymbol{K}}\cdot\boldsymbol{p}}{\left(\kappa^2+\boldsymbol{\pi}_0^2\right)^2}\delta(Q). \tag{B3}$$

Here we have substituted the definition of Q [Eq. (10)]. Representing now $\boldsymbol{\varepsilon}_{\boldsymbol{K}}$ as in Eq. (18) and also $\boldsymbol{p}=|\boldsymbol{p}|\boldsymbol{n}_{\boldsymbol{p}}$, as well as substituting the definition of the constant $\mathcal{N}$ from Eq. (23), we arrive at

$$\mathcal{A}_{\rm FF}=2\pi\mathcal{N}|\boldsymbol{p}|\delta(Q)\mathcal{R}_\delta^{(0)}, \tag{B4}$$

with $\mathcal{R}_\delta^{(0)}$ given by Eq. (19).

APPENDIX C: COMBLIKE STRUCTURES IN LASER-INDUCED AND LASER-ASSISTED PROCESSES

As explained in Sec. II, there is a significant difference in the theoretical treatment of laser-induced and laser-assisted

processes. The difference comes from the fact that laser-assisted processes can happen even in the absence of the field, which is not the case for laser-induced processes. As argued in the main text, the probability amplitude of a laser-assisted process has field-modified and field-induced contributions, both of which have to be accounted for. It is the latter that can exhibit coherent comb structures, as we show below. Note that the same is applicable to laser-induced processes.

Consider the probability amplitude of a quantum process involving the train of $N_{\rm rep}$ identical laser pulses, each of duration τ_p,

$$\mathcal{A}_{N_{\rm rep}} = \int_0^{N_{\rm rep}\tau_p} dt\, G(t) e^{iQt + iH(t)}, \tag{C1}$$

where Q is a constant and $H(t) = \int_0^t d\tau\, h(\tau)$. We assume that the function $G(t)$ is continuous and satisfies the condition

$$G(0) = G(\tau_p) = 0. \tag{C2}$$

Moreover, it is repeated $N_{\rm rep}$ times. The same concerns the function $h(t)$. In contrast, $H(t)$ is not changing repeatedly over the duration of the train. However, the function $H_{\rm osc}(t)$ defined such that

$$H_{\rm osc}(t) = \int_0^t d\tau [h(\tau) - D], \tag{C3}$$

where

$$D = \frac{1}{\tau_p}\int_0^{\tau_p} d\tau\, h(\tau) = \frac{H(\tau_p)}{\tau_p}, \tag{C4}$$

already is. It also satisfies the condition

$$H_{\rm osc}(0) = H_{\rm osc}(\tau_p) = 0. \tag{C5}$$

Keeping in mind these definitions, we represent (C1) as

$$\mathcal{A}_{N_{\rm rep}} = \int_0^{N_{\rm rep}\tau_p} dt\, G(t) e^{i(Q+D)t + iH_{\rm osc}(t)}. \tag{C6}$$

Dividing this integral into the sum of integrals as

$$\mathcal{A}_{N_{\rm rep}} = \sum_{K=1}^{N_{\rm rep}} \int_{(K-1)\tau_p}^{K\tau_p} dt\, G(t) e^{i(Q+D)t + iH_{\rm osc}(t)} \tag{C7}$$

and shifting the variable of integration in each of them by $(K-1)\tau_p$, we conclude that

$$\mathcal{A}_{N_{\rm rep}} = \mathcal{A}_1 \sum_{K=1}^{N_{\rm rep}} e^{i(K-1)(Q+D)\tau_p}, \tag{C8}$$

where $\mathcal{A}_1$ is defined by Eq. (C1) if $N_{\rm rep} = 1$. Summing the above geometric series gives

$$\mathcal{A}_{N_{\rm rep}} = \mathcal{A}_1 e^{(i/2)(Q+D)(N_{\rm rep}-1)\tau_p} \frac{\sin\left[\frac{1}{2}(Q+D)N_{\rm rep}\tau_p\right]}{\sin\left[\frac{1}{2}(Q+D)\tau_p\right]}. \tag{C9}$$

As one can see, the probability amplitude of a process involving the train of pulses scales like the one for a single pulse but it is modulated (up to the overall phase factor) by the characteristic interference factor. The latter is given by the term with the sine functions. It follows from this formula that the probability amplitude takes maximum values when

$$\tfrac{1}{2}(Q+D)\tau_p = \pi N, \quad N \in \mathbb{Z}. \tag{C10}$$

In this case, the interference factor equals $N_{\rm rep}$. We therefore expect to observe the coherent $N_{\rm rep}^2$ enhancement of the respective probability distributions when the above condition is fulfilled. While the above considerations are the most general, in this paper we demonstrated how they relate to the field-induced contribution of the LARR process.

[1] K. C. Kulander, K. J. Schafer, and J. L. Krause, in *Super-Intense Laser-Atom Physics*, edited by B. Piraux, A. L'Huillier, and K. Rzążewski, NATO Advanced Studies Institute, Series B: Physics (Springer, Boston, 1993), Vol. 316, p. 95.

[2] P. B. Corkum, Phys. Rev. Lett. **71**, 1994 (1993).

[3] G. Farkas and C. Tóth, Phys. Lett. A **168**, 447 (1992).

[4] S. E. Harris, J. J. Macklin, and T. W. Hänsch, Opt. Commun. **100**, 487 (1993).

[5] F. Krausz and M. Ivanov, Rev. Mod. Phys. **81**, 163 (2009).

[6] A. Scrinzi, M. Y. Ivanov, R. Kienberger, and D. M. Villeneuve, J. Phys. B **39**, R1 (2006).

[7] F. Frank, C. Arrell, T. Witting, W. A. Okell, J. McKenna, J. S. Robinson, C. A. Haworth, D. Austin, H. Teng, I. A. Walmsley, J. P. Marangos, and J. W. G. Tisch, Rev. Sci. Instrum. **83**, 071101 (2012).

[8] U. Schramm, J. Berger, M. Grieser, D. Habs, E. Jaeschke, G. Kilgus, D. Schwalm, A. Wolf, R. Neumann, and R. Schuch, Phys. Rev. Lett. **67**, 22 (1991).

[9] U. Schramm, T. Schüssler, D. Habs, D. Schwalm, and A. Wolf, Hyperfine Interact. **99**, 309 (1996).

[10] I. D. Williams, J. McKenna, J. Wood, M. Suresh, W. A. Bryan, S. L. Stebbings, E. M. L. English, C. R. Calvert, B. Srigengan, E. J. Divall, C. J. Hooker, A. J. Langley, and W. R. Newell, Phys. Rev. Lett. **99**, 173002 (2007).

[11] E. S. Shuman, R. R. Jones, and T. F. Gallagher, Phys. Rev. Lett. **101**, 263001 (2008).

[12] T. Mohamed, G. Andler, M. Fogle, E. Justiniano, S. Madzunkov, and R. Schuch, Phys. Rev. A **83**, 032702 (2011).

[13] A. Jaroń, J. Z. Kamiński, and F. Ehlotzky, Phys. Rev. A **61**, 023404 (2000).

[14] M. Y. Kuchiev and V. N. Ostrovsky, Phys. Rev. A **61**, 033414 (2000).

[15] A. Jaroń, J. Z. Kamiński, and F. Ehlotzky, Phys. Rev. A **63**, 055401 (2001).

[16] D. B. Milošević and F. Ehlotzky, Phys. Rev. A **65**, 042504 (2002).

[17] C. Leone, S. Bivona, R. Burlon, and G. Ferrante, Phys. Rev. A **66**, 051403(R) (2002).

[18] T. Cheng, X. Li, S. Ao, L.-A. Wu, and P. Fu, Phys. Rev. A **68**, 033411 (2003).

[19] S. Bivona, R. Burlon, G. Ferrante, and C. Leone, Laser Phys. Lett. **1**, 118 (2004).
[20] S. Bivona, G. Bonanno, R. Burlon, and C. Leone, Phys. Rev. A **76**, 031402(R) (2007).
[21] C. Müller, A. B. Voitkiv, and B. Najjari, J. Phys. B **42**, 221001 (2009).
[22] A. N. Zheltukhin, A. V. Flegel, M. V. Frolov, N. L. Manakov, and A. F. Starace, J. Phys. B **45**, 081001 (2012).
[23] R. A. Müller, D. Seipt, S. Fritzsche, and A. Surzhykov, Phys. Rev. A **92**, 053426 (2015).
[24] A. Jaroń, J. Z. Kamiński, and F. Ehlotzky, J. Phys. B **34**, 1221 (2001).
[25] S. Odžak and D. B. Milošević, Phys. Rev. A **92**, 053416 (2015).
[26] A. Čerkić, M. Busuladžić, and D. B. Milošević, Phys. Rev. A **95**, 063401 (2017).
[27] A. Tutmić, A. Čerkić, M. Busuladžić, and D. B. Milošević, Eur. Phys. J. D **73**, 231 (2019).
[28] J. Z. Kamiński and F. Ehlotzky, Opt. Commun. **234**, 343 (2004).
[29] S. X. Hu and L. A. Collins, Phys. Rev. A **70**, 013407 (2004).
[30] J. Z. Kamiński and F. Ehlotzky, Phys. Rev. A **71**, 043402 (2005).
[31] J. Z. Kamiński and F. Ehlotzky, J. Mod. Opt. **53**, 7 (2006).
[32] S. Bivona, R. Burlon, G. Ferrante, and C. Leone, Opt. Express **14**, 3715 (2006).
[33] S. Bivona, R. Burlon, and C. Leone, Laser Phys. Lett. **4**, 44 (2007).
[34] A. Čerkić and D. B. Milošević, Phys. Rev. A **88**, 023414 (2013).
[35] L. V. Keldysh, Sov. Phys. JETP **20**, 1307 (1965).
[36] F. H. M. Faisal, J. Phys. B **6**, L89 (1973).
[37] H. R. Reiss, Phys. Rev. A **22**, 1786 (1980).
[38] A. J. Jerri, *The Gibbs Phenomenon in Fourier Analysis, Splines and Wavelet Approximations* (Springer, Dordrecht, 1998).
[39] J. J. Duistermaat and J. A. C. Kolk, *Distributions: Theory and Applications* (Springer, New York, 2010).
[40] G. F. Gribakin and M. Y. Kuchiev, Phys. Rev. A **55**, 3760 (1997).
[41] M. Boca and V. Florescu, Phys. Rev. A **80**, 053403 (2009).
[42] F. Cajiao Vélez, L. Geng, J. Z. Kamiński, L.-Y. Peng, and K. Krajewska, Phys. Rev. A **102**, 043102 (2020).
[43] L. Geng, F. Cajiao Vélez, J. Z. Kamiński, L.-Y. Peng, and K. Krajewska, Phys. Rev. A **102**, 043117 (2020).
[44] K. Krajewska and J. Z. Kamiński, Laser Phys. Lett. **11**, 035301 (2014).
[45] K. Krajewska, M. Twardy, and J. Z. Kamiński, Phys. Rev. A **89**, 052123 (2014).
[46] G. F. Boudreaux-Bartels, in *The Transforms and Applications Handbook*, 2nd ed., edited by A. D. Poularikas (CRC, Boca Raton, 2000).
[47] R. Kanya, Y. Morimoto, and K. Yamanouchi, Phys. Rev. Lett. **105**, 123202 (2010).
[48] Y. Morimoto, R. Kanya, and K. Yamanouchi, J. Chem. Phys. **140**, 064201 (2014).
[49] R. Kanya and K. Yamanouchi, Atoms **7**, 85 (2019).